J Appl Electrochem (2013) 43:721–734
DOI 10.1007/s10800-013-0562-1

ORIGINAL PAPER

Electrochemical properties of electrodeposited nanocrystalline cobalt and cobalt–iron alloys in acidic and alkaline solutions

N. M. Nik Rozlin · Akram M. Alfantazi

Received: 23 January 2013 / Accepted: 8 May 2013 / Published online: 17 May 2013

Abstract Nanocrystalline Co and CoFe with varied iron contents ranging from 5 to 25 wt% Fe were electrodeposited from a sulfate bath. The average grain sizes of the coatings obtained were measured using Scherrer equation and calculated to be in between 16 and 65 nm. Electrochemical corrosion behavior of electrodeposited nanocrystalline cobalt (Co) and cobalt–iron (CoFe) alloys was investigated in both acidic (0.1 M H_2SO_4) and alkaline solution (0.1 M NaOH). This study investigates the corrosion behavior of electrodeposited CoFe alloy coatings using polarization tests, electrochemical impedance spectroscopy, and X-ray photoelectron spectroscopy techniques. The nanocrystalline Co and CoFe showed active behavior for all alloy coatings in acidic condition, while an active–passive–transpassive behavior was seen for all coatings in alkaline condition.

Keywords Nanocrystalline CoFe · Corrosion · Potentiodynamic polarization · EIS · XPS

1 Introduction

Electrodeposition has been a popular choice in the production of alloys that require certain physical, mechanical, or chemical properties to be highlighted [1, 2]. Many studies have shown that various alloys have successfully been electrodeposited to exhibit enhanced mechanical and electrochemical properties. Electrodeposited Zn–Ni with Ni varying between 8 and 14 % has resulted in five to six times lower corrosion rates and better physical properties when compared to pure Zn [3–6]. The addition of phosphorus to electrodeposited cobalt has also been shown to increase corrosion resistance [7, 8].

Nanocrystalline coatings produced from electrodeposition are also gaining tremendous attention due to their potential in various applications. In order to further expand their capabilities and future applications, their corrosion resistance in aqueous solution is of great importance. Corrosion not only changes the properties of these nanocrystalline coatings but also decrease their service life. Several researches have both reported on the positive and negative effects of nanocrystallization of materials on their corrosion behavior. Due to changes in surface area, the activity of the metallic atom determines the corrosion properties of the nanomaterials. The high volume fraction of grain boundaries results in different corrosion performance among various metals and corrosion environment. Corrosion rate increases due to soluble corrosion products in the electrochemical solution, while insoluble corrosion products increases corrosion resistance which act as a barrier to prevent active dissolution, hence, decreases the corrosion rate.

Recently, there has been interest in electrodepositing Co with Fe to produce CoFe alloy coatings due to their excellent magnetic properties. These alloys have found many applications in magnetic recording (read/write heads) and ultra large scale integration (ULSI) devices [9, 10]. Moreover, it has also been incorporated into microelectromechanical (MEMS) devices such as sensors, microactuators, microgears, and micromotors [11]. This is mainly due to their low magnetic loss, high saturation magnetic flux density, low coercive force, and high permeability.

N. M. Nik Rozlin (✉) · A. M. Alfantazi
Department of Materials Engineering, The University of British Columbia, 6350 Stores Road, Vancouver, BC V6T1Z4, Canada
e-mail: nikrozlin@yahoo.com

A. M. Alfantazi
e-mail: akram.alfantazi@ubc.ca

However, the literature on electrodeposited CoFe has focused mainly on their magnetic behavior [12–15]. In order to develop the range of future applications for this promising alloy, it is crucial to understand and determine its electrochemical behavior. A study by Ricq et al. [16] investigated the influence of sodium saccharin on the electrodeposition process as well as the corrosion of CoFe deposits. The results showed that corrosion resistance decreases in deposits obtained from solutions containing high concentration of sodium saccharin. The authors concluded that the poor corrosion behavior was due to the high sulfur content in the alloy coating. The effect of saccharin on the corrosion behavior of CoFe was also investigated by Tabakovic et al. [17]. The electrochemical properties of electroplated CoFe were compared with sputtered CoFe. Similar conclusions to those of Ricq et al. [16] were drawn viz. that electroplated CoFe had lower corrosion resistance due to the sulfide present at grain boundaries. This enhanced the anodic dissolution and hindered passivation. George et al. [18] also conducted a study on sulfur and saccharin incorporation into electrodeposited CoFe, and they too have concluded that the presence of sulfur leads to higher corrosion susceptibility.

It can be seen that previous studies have focused on the effect of saccharin on the corrosion behavior of electrodeposited CoFe. Furthermore, their electrochemical properties in different pH solutions are also very limited. Thus, this study aims to investigate the effect of iron content on the corrosion behavior of electrodeposited nanocrystalline CoFe alloy coatings in both acidic and alkaline environments. Potentiodynamic polarization was used to study the electrochemical corrosion behavior of the alloy deposits, while electrochemical impedance spectroscopy (EIS) was employed in order to gain information on the possible interactions taking place at the solid/liquid interface of the samples. The CoFe alloy coatings will be compared to pure nanocrystalline Co to study the effect of iron addition.

2 Experimental procedure

2.1 Electrodeposition of nanocrystalline Co and CoFe alloy coatings

CoFe deposits were synthesized from a sulfate solution. A standard three-electrode cell configuration was used to synthesize nanocrystalline CoFe films. Titanium was used as the cathode substrate with an exposed area of 1 cm^2, and the anode material was a graphite rod placed 20 cm from the cathode. The substrate was bonded to a copper wire using a conductive silver epoxy to establish an electrical connection. Prior to electrodeposition, the titanium substrate was ground with silicon carbide papers of 240, 320, 600, 800, and 1,200 grit, polished with 1 μm alumina powder and then rinsed with distilled water. The substrate was then immersed in sulfuric acid for a few seconds to eliminate all contaminants. Specimens were weighed before and after the electrodeposition process.

The plating bath for CoFe deposits consisted of cobalt sulfate (250×10^3 mg L^{-1}), iron sulfate (10×10^3–80×10^3 mg L^{-1}), sodium sulfate (25×10^3 mg L^{-1}), boric acid (30×10^3 mg L^{-1}), and saccharin (1.5×10^3 mg L^{-1}). Boric acid and saccharin were added as a pH buffer and grain refiner, respectively. Iron sulfate concentration was adjusted to produce CoFe deposits with various iron contents. All chemicals were reagent grade and immersed in distilled water. The temperature of the bath was maintained at 40 °C by employing a water bath, and the solution was continuously stirred using a magnetic stirrer. Sulfuric acid (H_2SO_4) or sodium hydroxide (NaOH) was added in small drops to the electrolyte bath in order to adjust the pH of the bath solution to 2.5. During the electrodeposition process, direct current of 3×10^3 mA cm^{-2} was applied. The deposits were immediately taken out from the solution after the plating process and washed under running water for several minutes to remove any contaminants. All deposits were then dried with hot air and mechanically stripped from the substrate for further analysis. A number of pure nanocrystalline Co deposits were produced from cobalt sulfate (250×10^3 mg L^{-1}), boric acid (40×10^3 mg L^{-1}), and saccharin (1.5×10^3 mg L^{-1}) to compare the corrosion behavior of nanocrystalline CoFe alloy coatings. The thickness of these alloys was determined by using the SEM and was measured to be about 60–70 μm.

2.2 Characterization

The scanning electron microscope (SEM) Hitachi S-3000N was used to characterize the microstructure of nanocrystalline CoFe alloy coatings. Energy dispersive X-ray spectroscopy (EDS) Hitachi S-3000N and Electron Probe Micro Analyzer (EPMA) CAMECA SX-50 instrument were used to determine the chemical composition of the nanocrystalline coatings. X-ray diffraction (XRD) was performed on Siemens D5000 X-ray diffractometer using Cu Kα radiation (40 kV, 20 mA). The 2θ ranged from 10° to 70° with a step width of 0.04°. The average grain size of crystallites was calculated from the line broadening of the X-ray peaks using the Scherrer formula. The Hitachi H800 transmission electron microscopy (TEM) was also used to determine the accuracy of the grain size measurements of the coatings. The surface morphology of all samples after the potentiodynamic polarization test was examined using the Hitachi S-3000N SEM. The chemical composition on the surface of samples was analyzed automatically by a Leybold MAX2000 XPS spectrometer using a monochromatic Mg Kα X-ray source and pass energies of 192 and

48 eV for wide and high-resolution scans, respectively. The at.% of elements present on the coatings surface from the XPS spectrum is measured by using the XPS instrument where the position of the peaks in the spectrum allows identification of atomic composition present on the samples surface and hence allows the composition of the elements to be determined quantitatively.

2.3 Electrochemical testing

A conventional three-electrode cell was used which consisted of graphite as the counter electrode, saturated calomel electrode (SCE) as the reference electrode, and nanocrystalline Co or CoFe alloy coatings that were mechanically removed from the Ti substrate as the working electrode. The corrosion experiments for the nanocrystalline CoFe were conducted in deaerated 0.1 M H_2SO_4 (pH 1) and 0.1 M NaOH (pH 13) using the potentiodynamic polarization. The solutions were deaerated by purging argon gas throughout the experiments. Electrodeposited CoFe alloy coating with different iron contents of 5, 11, and 25 wt% was used for the electrochemical tests. Prior to corrosion testing, all specimens were ultrasonically cleaned, degreased with acetone, and rinsed thoroughly with deionized water. The specimens were then mounted in a PTFE holder with an exposed area of 1 cm^2. All electrochemical measurements were carried out with a Princeton Applied Research Versastat 4 potentiostat. The open circuit potential (OCP) measurement was carried out to allow the working electrode to reach a steady state. The potentiodynamic polarization measurements were performed from −500 mV versus OCP to 800 mV versus SCE with a scan rate of 0.5 mVs^{-1} in acidic solution and 1 mVs^{-1} in alkaline solution. All potentials reported in the present work are reported versus SCE. All tests were carried out at room temperature (25 °C). Impedance measurement was carried out in the frequency range from 10 kHz to 10 mHz with an ac voltage amplitude of 5 mV. A commercial software ZSimpWin^{TM} was used to interpret the measured frequency response using a nonlinear least-square fitting procedure.

3 Results and discussion

3.1 Chemical composition, grain size, and surface morphology of CoFe alloy coatings

Iron sulfate in the amount ranging from 10×10^3 to 80×10^3 mg L^{-1} was used to produce CoFe alloy coatings with different iron contents. EDS and EPMA analysis showed that the Fe content of the deposits ranges from 5 to 25 wt%. The average grain sizes of the coatings obtained with different iron content were measured using Scherrer equation and calculated from the line broadening of the X-ray peaks from XRD. Interestingly, in our earlier study, it was found that the grain sizes of the deposited alloys decreased with addition of iron [19]. The obtained chemical composition and grain size of the nanocrystalline Co and CoFe alloy coatings are listed in Table 1. Figure 1a, b shows the TEM micrographs of Co–11Fe and Co–25Fe, respectively, which further confirm the existence of the fine grains in the CoFe deposit. The average grain size of Co–25Fe alloy coating was about 18 nm. By direct measurement from the TEM micrograph, the grain size of the Co–25Fe coating was found in the range of 10–70 nm and the calculated average grain size was about 20 ± 5 nm which was close to the value obtained from the Scherrer formula of about 18 nm. This shows that the Scherrer method is a reliable method to calculate the average grain size of the deposits. The SEM surface morphology of the nanocrystalline Co and CoFe alloy coatings is shown in Fig. 2. From the figure, it can be seen that all coatings were smooth, compact, and uniform. The morphology of nanocrystalline Co changed from acicular to spherical with homogeneous size distribution and smooth surface grains with the addition of Fe in the alloy coatings.

Table 1 Iron composition and grain size of nanocrystalline Co and CoFe alloy

Coatings	Fe content (wt%)	Average grain size (nm)
Co	0	65
Co–5Fe	5.36	56
Co–11Fe	11.42	38
Co–25Fe	25.18	16

3.2 Acidic conditions

3.2.1 Open circuit potential measurements in 0.1 M H_2SO_4

The open circuit potential (OCP)-time behavior was measured for nanocrystalline Co and CoFe alloys and is shown in Fig. 3. The OCP for pure Co decreased from −400 mV_{SCE} for the first 3 min that could be attributed to the anodic dissolution of air-formed oxide film before it stabilizes at the value of −410 mV_{SCE}. Meanwhile, addition of iron to pure cobalt decreased the OCP value further. This indicates active dissolution of the Fe which implies a deterioration of corrosion resistance of the alloy coating. The OCP value decreased from −417 to −440 mV_{SCE} with an increase in iron content ranging from 5 to 25 wt% Fe of the nanocrystalline CoFe deposits.

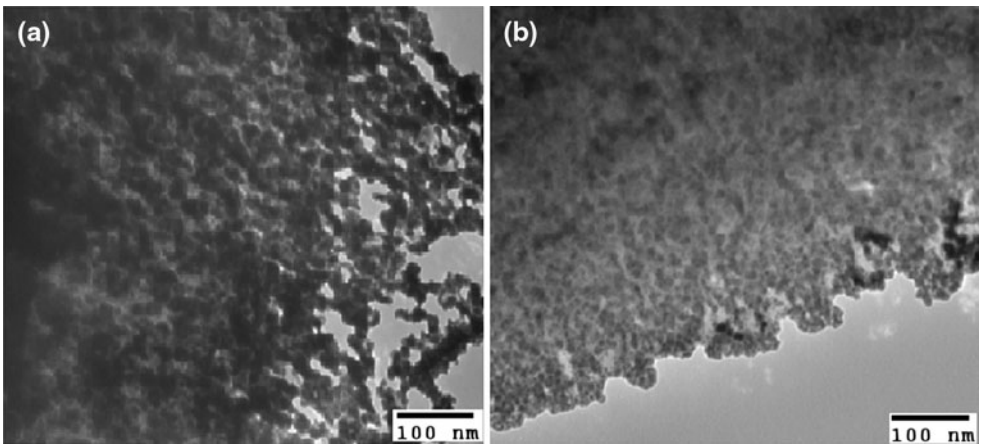

Fig. 1 TEM images of CoFe alloy electrodeposited with different iron contents. **a** 11 wt% Fe and **b** 25 wt% Fe

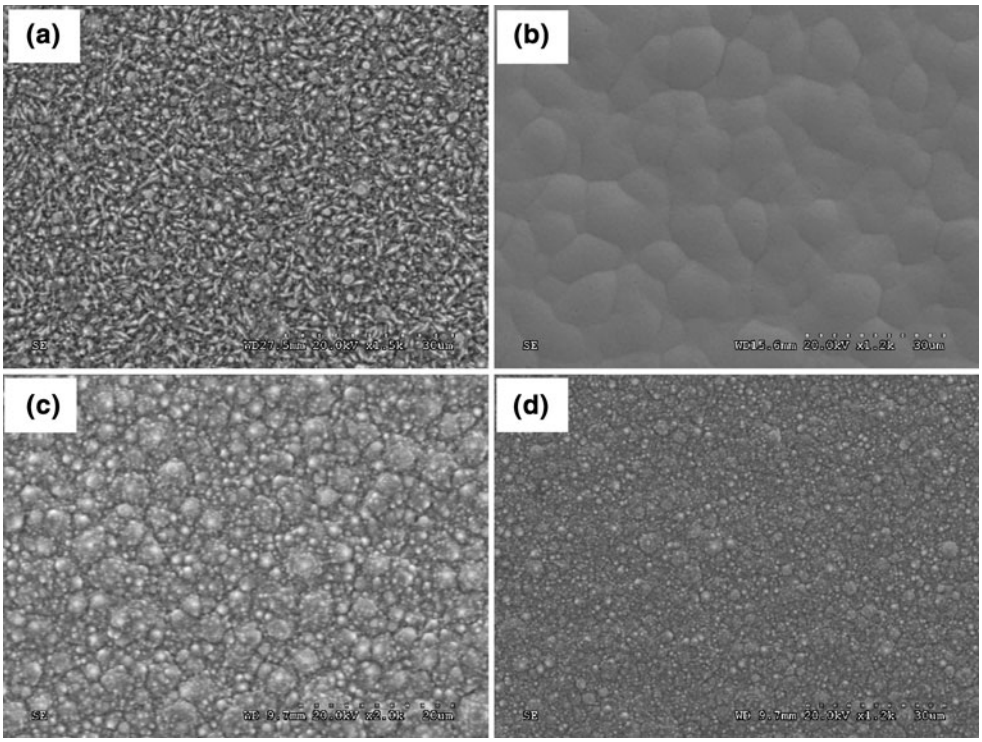

Fig. 2 SEM images of CoFe alloy electrodeposited with different iron contents. **a** 100 wt% Co, **b** 5 wt% Fe, **c** 11 wt% Fe, **d** 25 wt% Fe

3.2.2 Potentiodynamic polarization in 0.1 M H_2SO_4

Figure 4 illustrates the potentiodynamic polarization behavior of nanocrystalline Co and CoFe alloys with different iron content in deaerated 0.1 M H_2SO_4 with a scan rate of 1 mVs^{-1}. The scan was started at the cathodic potential in order to reduce air-formed oxides on the electrode surface and was further continued until a high upper threshold potential of 1×10^3 mV_{SCE}. One of the concerns about scanning to high potentials is the electrolyte conductivity and the corresponding IR drop. However, in these experiments, the reference electrode was always positioned at a fixed distance of 0.5 cm from the working electrode. Also, based on the conductivity of the solution, 8.9 (mS cm^{-1}), the maximum current density of 50 mA cm^{-2}, and the sample area of 1 cm^2, the maximum contribution of the IR drop in the applied potential was calculated to be below 2.8×10^{-5} and so is negligible.

From the potentiodynamic polarization experiment, typical anodic and cathodic polarization curves were observed. All samples exhibit active dissolution without any distinctive transition to passivation within the applied potential range. It is also apparent that Co coating exhibited a mass transfer limit which was reached at about 0 mV_{SCE},

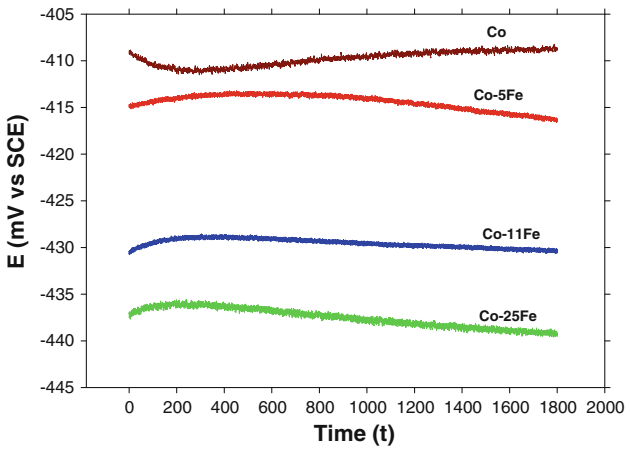

Fig. 3 Eoc time behavior of CoFe alloys with various iron content in 0.1 M H_2SO_4

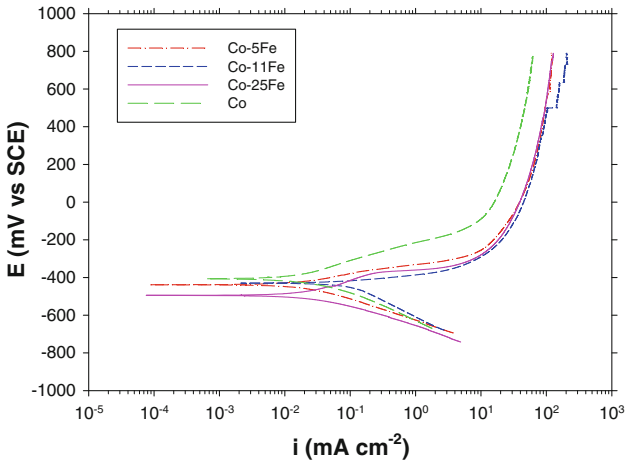

Fig. 4 Potentiodynamic polarization curves of CoFe with various iron content in deaerated 0.1 M H_2SO_4 with a scan rate of 0.5 mVs^{-1}

while CoFe alloy coatings exhibited a much lower limit. Similar results were obtained [20, 21] where only active dissolution was present in acidic environment. It can be seen that the effect of alloying Fe to electrodeposited Co led to an increase in the kinetics of the anodic metal dissolution which moved the corrosion potential (E_{corr}) to a more negative value and increased corrosion current. The possible anodic reactions are [22]:

$$Fe + (FeOH)_{ads} \rightarrow Fe(FeOH)_{ads} \quad (1)$$

$$Fe(FeOH)_{ads} + OH^- \rightarrow FeOH^+ + (FeOH)_{ads} + 2e^- \quad (2)$$

$$FeOH^+ + H^+ \rightarrow Fe^{2+} + H_2O \quad (3)$$

Electrochemical parameters obtained from potentiodynamic polarization are listed in Table 2. It can be observed that all nanocrystalline CoFe deposits show more negative corrosion potentials as compared to pure Co sample. Nanocrystalline CoFe with the least iron content of about 5 wt% Fe had a corrosion potential of −476 mV_{SCE}, while electrodeposits containing higher iron content of 11 and 25 wt% Fe showed slightly more negative corrosion potentials of −474 and −495 mV_{SCE}, respectively. It has been reported that further increase in Fe content reduced the grain sizes of CoFe coatings [19]. This grain refinement provides a greater surface area of active sites that leads to the acceleration of the kinetics of the anodic reaction through the formation of more electrochemical corrosion cells. It is well known that grain sizes in the nanocrystalline range enhance corrosion activity due to the large number of grain boundaries available for preferential attack sites in corrosive environments. Hence, it is expected that corrosion resistance decreases with increasing Fe content due to the grain refining of the alloy deposits. This detrimental effect of high iron content on the corrosion behavior of CoFe coatings in acidic solutions could be further seen through the corrosion current density obtained from the extrapolation of the Tafel slopes as shown in Table 2. The corrosion current density increased from 0.036 to 0.057 mA cm^{-2} with the addition of iron (5–11 wt% Fe) into the nanocrystalline Co coatings. Furthermore, the increase in corrosion rate for these nanocrystalline CoFe alloy coatings maybe due to the effect of the saccharin used in the plating bath during the deposition process. Several studies [17, 18, 23] have reported that the use of saccharin in electroplating CoFe could reduce the corrosion resistance of the alloy coatings due to the presence of sulfur in the metal surface. A study by Oudar [24] had also mentioned the negative effect of absorbed sulfur on the metal surface which further accelerated the anodic dissolution due to the weakening between the metal–metal bonds. Hence, the addition of saccharin as a grain refiner in the plating solution in the present study could possibly contribute to the decrease in corrosion resistance of the CoFe coatings. However, further investigations on the amount of sulfur present on the surface alloy coating have to be carried out in order to verify and confirm the effect of sulfur on the corrosion properties of CoFe coatings.

3.2.3 *Electrochemical impedance spectroscopy (EIS) in 0.1 M H_2SO_4*

EIS was performed on both pure Co and CoFe alloy coatings to provide insight into the electrochemical process occurring at the sample surface and solution interface. Nyquist plots for both Co and CoFe alloys in 0.1 M H_2SO_4 are shown in Fig. 5. From the plots obtained, it can be seen that for Co and CoFe alloy coatings, two loops could be distinguished for both types of nanocrystalline coatings. The first loop at high-frequency region appears as a capacitive loop which belongs to a double layer

Table 2 Potentiodynamic polarization data of Co and CoFe alloys in 0.1 M H_2SO_4

Coating	E_{corr} (mV_{SCE})	β_a ($mVdec^{-1}$)	β_c ($mVdec^{-1}$)	I_{corr} ($mA\ cm^{-2}$)
Co	−420.89	120	141	0.021
Co–5Fe	−465.74	123	145	0.036
Co–11Fe	−473.66	125	147	0.048
Co–25Fe	−494.55	129	149	0.057

capacitance parallel to charge transfer resistance. At the lower frequencies, an inductive loop was observed. It has been reported that the low-frequency loop was attributed to a slow reaction during metal dissolution process and surface coverage by hydrogen [20, 25]. The EIS results were fitted with an equivalent circuit that involves a double layer capacitance, charge transfer resistance, and an element to represent adsorption. The electrical circuit parameters were simulated using the software package ZSimpWin. The typical chi-square values were less than 5×10^{-4} indicating a satisfactory fit. The proposed equivalent circuit is shown in Fig. 6. It consists of a working electrode (W_E), solution resistance (R_s) in series with a double layer capacitance (Q_{dl}), charge transfer resistance (R_{ct}), adsorption capacitance (Q_a), and the adsorption resistance (R_a). Table 3 presents the values obtained by the best fit to the equivalent circuit model. It can be seen from Table 3 that pure Co coatings had the highest charge transfer resistance, while Co 25 wt% Fe had the lowest charge transfer resistance of 87 and 51 $\Omega\ cm^2$, respectively. This indicates better corrosion resistance for pure Co as compared to CoFe alloy coating in acidic environment. This further confirms the results obtained from the polarization test discussed earlier where the corrosion current density of the CoFe alloy obtained was higher indicating lower corrosion resistance as compared to pure Co deposits.

3.2.4 X-ray photoelectron spectroscopy analysis

XPS was carried out to determine the composition and chemical state of the nanostructured coatings. Figure 7a, b shows the survey (full-range) XPS spectrum of as-deposited Co and CoFe alloy coating and the polarized coatings obtained after potentiostatic treatment at −300 mV_{SCE} for 10 min, respectively. Cobalt, oxygen, carbon, sulfur, and iron elements were detected on both as-deposited and polarized CoFe alloy, while no Fe was detected for all Co samples as expected. The spectra obtained could be deconvoluted into sets of spin-orbit doublets together with satellite peaks [26]. Figure 8 shows the high-resolution XPS spectra of Co $2p_{3/2,1/2}$ where two peaks with binding

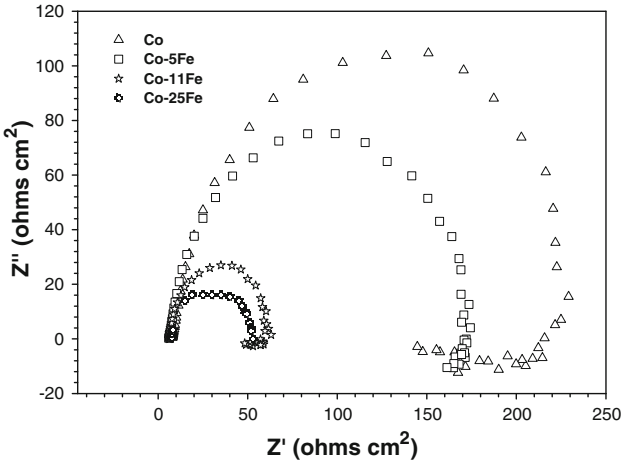

Fig. 5 Nyquist plots for nano Co and CoFe alloys with various iron content in deaerated 0.1 M H_2SO_4

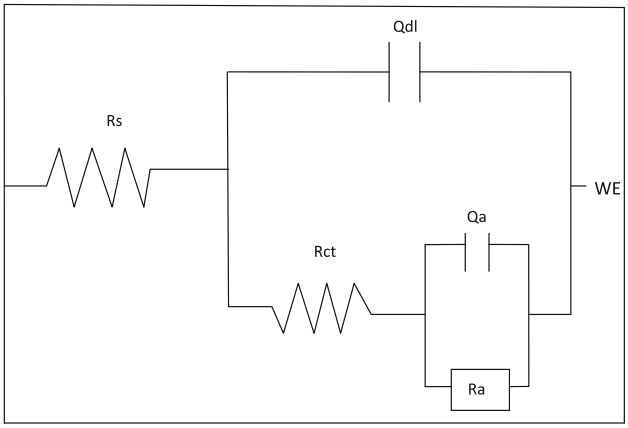

Fig. 6 Equivalent circuit proposed for the electrochemical impedance response of Co and CoFe alloy coatings in 0.1 M H_2SO_4

Table 3 EIS data obtained by equivalent circuit simulation in 0.1 M H_2SO_4

Coating	R_s ($\Omega\ cm^2$)	Q_{dl}–Y_o ($F\ cm^{-2}$)	n_1	R_{ct} ($\Omega\ cm^2$)
Co	8.165	0.0001200	0.9137	87
Co–5Fe	6.132	0.0001451	0.9581	77
Co–11Fe	5.655	0.0001677	0.8000	58
Co–25Fe	5.101	0.0001554	0.8215	51

energies of 781.3 ± 0.1 and 798.0 ± 0.1 eV are observed. These peaks could be attributed to the $Co(OH)_2$ [27] according to their satellite peak positions at 787.4 and 803.3 eV, respectively. These satellite peaks occur due to the shake-up phenomenon from unpaired valence electrons that gives rise to the number of relaxed final states [26]. Moreover, it can also be clearly seen that there is a significant increase in the ratio of cobalt oxides present for Co 25 wt% Fe alloy coatings after polarization as compared to the as-deposited coatings, while the ratio of cobalt oxides

for both as-deposited and polarized Co remain almost unchanged. Similar species were also reported in the literature for polarized nanocrystalline Co in H_2SO_4 [21]. Meanwhile, in Fig. 9, O 1 s peaks for samples polarized in 0.1 M H_2SO_4 were composed of three peaks at 530.1 ± 0.2, 531.4 ± 0.2, and 532.5 ± 0.2 eV which corresponded to O^{2-} ions, OH^- ions, and H_2O, respectively [28]. On the other hand, iron peaks were only detected from the CoFe alloy coatings. The high-resolution XPS spectrum of Fe 2p is shown in Fig. 10. One strong peak was observed at a binding energy of 713.1 ± 0.1 eV and another peak at 726 eV ± 0.1 eV which was found to correspond to Fe^{3+} [29]. It is interesting to note that the XPS spectrum of Fe was not detected from the corrosion film of Co 5 wt% Fe coating. This is probably attributed to the dissolution of the small amount of Fe in the acidic medium. However, Fe peaks were detected in CoFe coatings with higher Fe contents of 11 and 25 wt% Fe. Table 4 shows the atomic concentration ratio obtained from the XPS survey spectrum.

3.2.5 *Corrosion morphologies*

Figure 11 shows the SEM images of nanocrystalline Co and CoFe alloy coatings after potentiodynamic polarization in 0.1 M H_2SO_4. Different morphologies could be seen from both nanocrystalline Co and CoFe deposits. A smoother and more uniform corrosion product is present for nanocrystalline Co (Fig. 11a). Meanwhile, it can be observed that nanocrystalline CoFe coatings with 5 and 11 wt% Fe (Fig. 11b, c) exhibit an etch-pit like morphology. Larger and more enhanced pits indicating high anodic dissolution could be observed on CoFe coatings with the highest iron content as shown in Fig. 11d. This indicates a less protective surface film of the nanocrystalline CoFe alloy coatings in 0.1 M H_2SO_4 solution as compared to

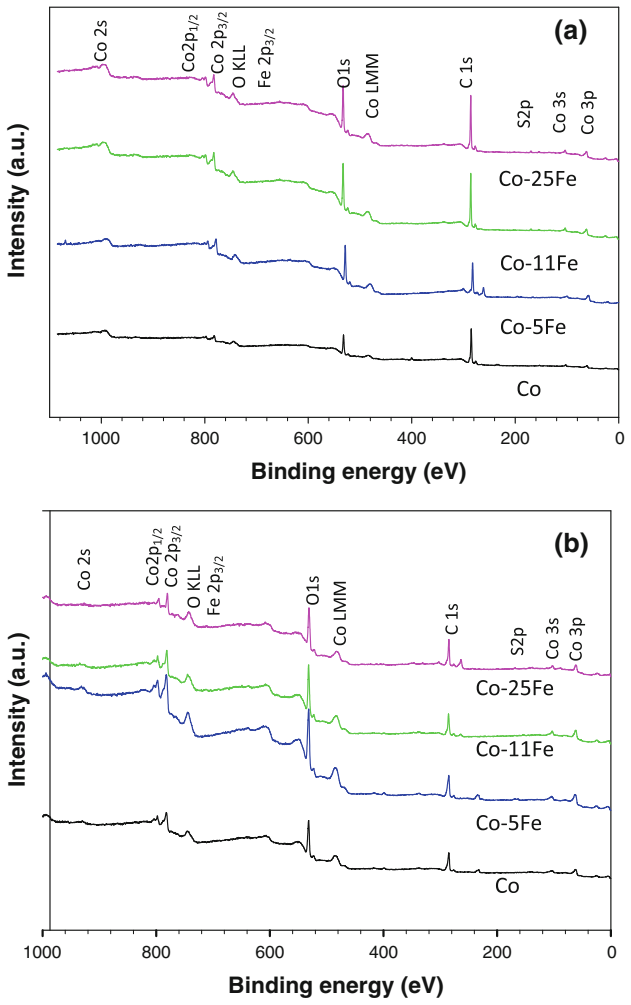

Fig. 7 XPS spectra (full-range) of **a** as-deposited and **b** nano Co and CoFe with various iron content in 0.1 M H_2SO_4 after potentiostatic treatment at −300 mV_{SCE} for 10 min

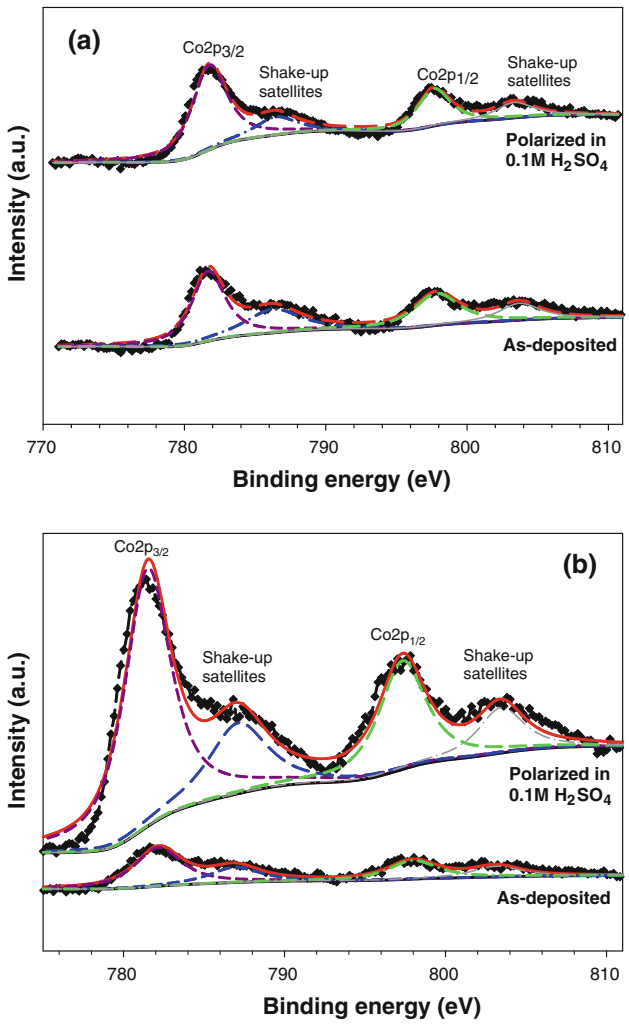

Fig. 8 Comparison of Co 2p peaks of **a** as-deposited Co and Co after polarization in 0.1 M H_2SO_4 and **b** as-deposited and Co 25 wt% Fe after polarization in 0.1 M H_2SO_4

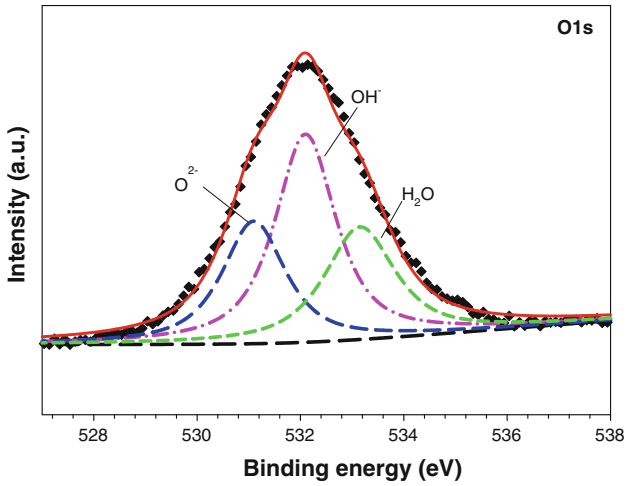

Fig. 9 Measured high-resolution spectra of O 1 s after polarization in 0.1 M H_2SO_4

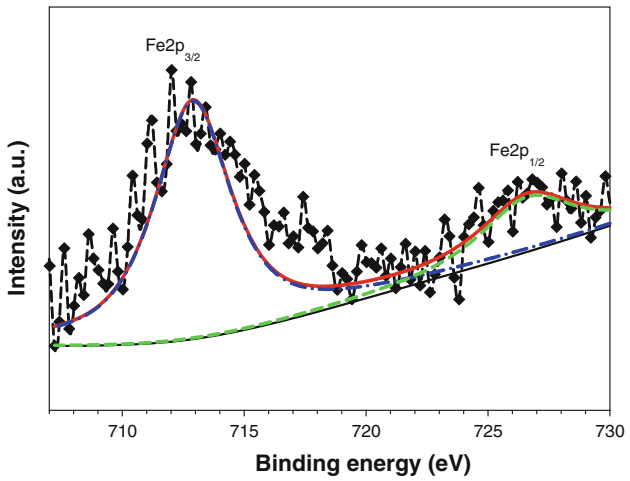

Fig. 10 Measured high-resolution spectra of Fe 2p of the Co 25 wt% Fe alloy coating after polarization in 0.1 M H_2SO_4

pure Co coating. Studies [30, 31] have also observed similar conditions of reduced corrosion resistance in acidic environments for nanocrystalline Ni–P alloys and Co, respectively. It is known that in nanostructured materials, the grain boundaries are usually sites for preferential attack when in contact with a corrosive environment. The high volume of grain boundaries in nanocrystalline materials could form large number of micro-electrochemical cells during the electrochemical process and provide more active sites to participate in corrosion reaction. The decline in corrosion resistance of nanocrystalline CoFe alloy coatings was attributed to the higher kinetics of the anodic dissolution on active sites. Since the density of grain boundaries is very high in nanocrystalline CoFe alloy, the electrochemical process is accelerated, hence, resulting in severe corrosion condition of the coating surface.

3.3 Alkaline condition

3.3.1 Open circuit potential measurements in 0.1 M NaOH

The open circuit potential with time for all Co and CoFe alloy coatings is shown in Fig. 12. The OCP variations in 0.1 M NaOH show similar characteristics for all samples. Co and CoFe (5 wt% Fe and 25 wt% Fe) display an instantaneous shift of potential toward positive values, which most probably corresponds to the growth of a surface film on the coatings. However, for Co 11 wt% Fe, the displacement of OCP toward more noble values was not immediate but started to shift and stabilize after a few minutes.

3.3.2 Potentiodynamic polarization in 0.1 M NaOH

Polarization tests were carried out on both Co and CoFe alloy coatings in an alkaline medium. The scan was started from a cathodic potential range and continued in the positive direction. The potential was swept up to 1×10^3 mV_{SCE} in order to make sure the passive region is past. Figure 13 shows a typical potentiodynamic polarization curve obtained from nanocrystalline Co and CoFe deposits in deaerated 0.1 M NaOH with a scan rate of 1 mVs^{-1} at room temperature. It can be observed that the curves of all samples have generally similar behavior. A typical active–passive–transpassive behavior is obtained for all tested samples where two stages of passivation could be observed at two different electrode potentials of −700 and 200 mV_{SCE}, respectively. Studies [7, 32] have also reported similar corrosion behavior for Co coatings. The appearance of two passivation stages has been reported to

Table 4 Atom concentration ratio (at.%) of elements in XPS analysis for as-deposited samples and polarized in 0.1 M H_2SO_4

Element	As-deposited				Polarized in 0.1 M H_2SO_4			
	Co	Co–5Fe (at.%)	Co–11Fe (at.%)	Co–25Fe (at.%)	Co	Co–5Fe (at.%)	Co–11Fe (at.%)	Co–25Fe (at.%)
Co	9.12	5.87	6.02	1.51	8.17	10.97	8.06	6.08
Fe	–	0.43	0.60	0.82	–	–	0.10	0.20
O	23.88	31.00	26.82	13.7	39.52	43.71	44.56	44.62
S	1.01	0.87	0.93	0.22	1.30	0.51	1.03	0.86

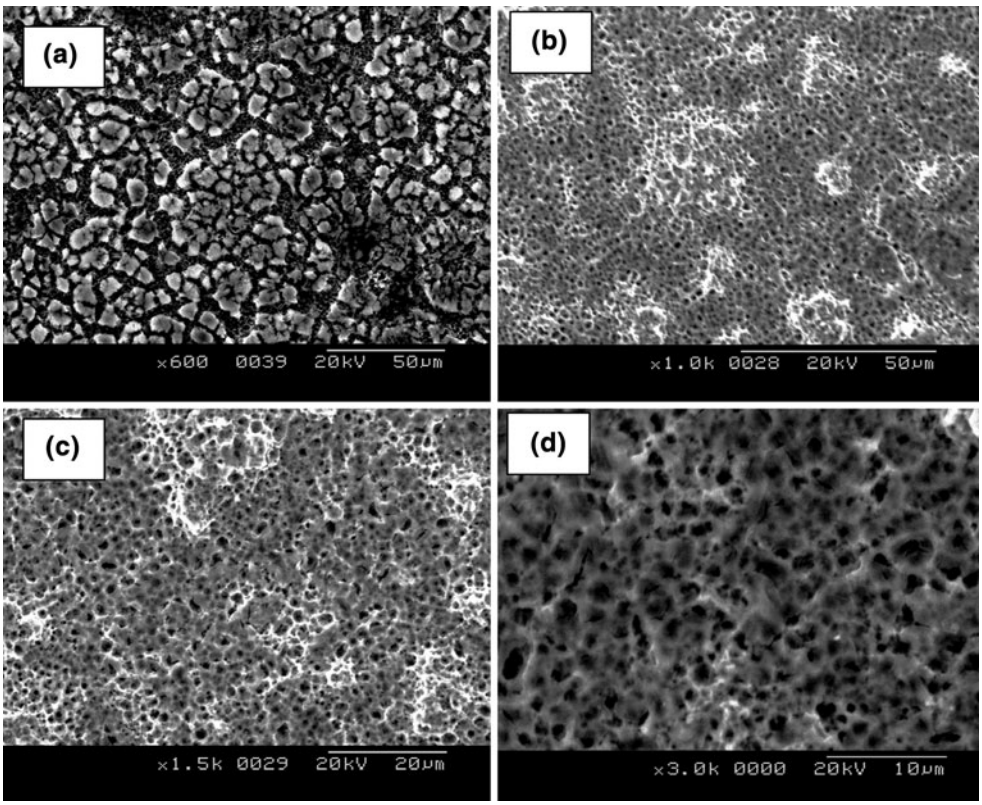

Fig. 11 SEM morphologies of the CoFe alloy coatings after potentiodynamic polarization test in deaerated 0.1 M H_2SO_4 **a** Co, **b** Co 5 wt% Fe, **c** Co 11 wt% Fe, **d** Co 25 wt% Fe

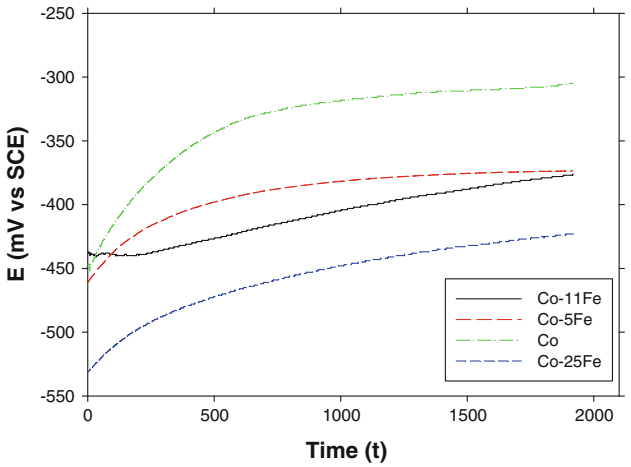

Fig. 12 Eoc time behavior of Co and CoFe alloys with various iron content in 0.1 M NaOH

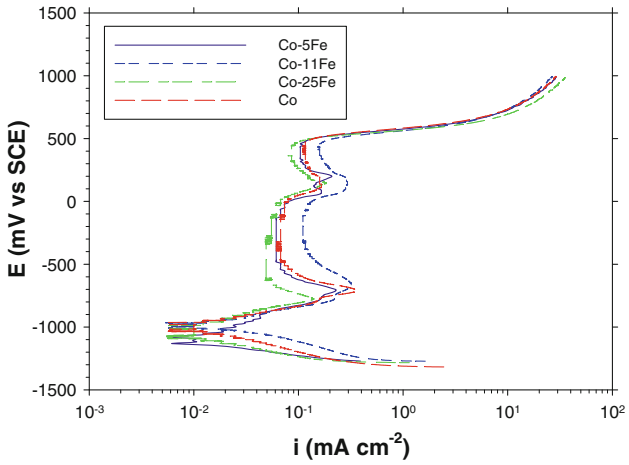

Fig. 13 Potentiodynamic polarization curves of Co and CoFe with various iron content in deaerated 0.1 M NaOH with a scan rate of 1 mVs^{-1}

be due to the formation of a duplex passive film. The duplex passivation film formed was reported to mainly consist of $Co(OH)_2$ on the primary passivation stage, while a rather complex compound of Co_3O_4/Co_2O_3 was identified on the second passivation stage. Although Fe was also present in the alloy coatings, the small amount as compared to Co content did not exhibit any obvious effect on the passivation behavior. Table 5 summarizes the corrosion

Table 5 Potentiodynamic polarization data of CoFe alloys in 0.1 M NaOH

Coating	E_{corr} (mV)	β_a ($mVdec^{-1}$)	β_c ($mVdec^{-1}$)	I_{corr} (mA cm^{-2})
Co	−1,010	52.9	82.2	0.00883
Co–5Fe	−1,080	196.2	91.6	0.00644
Co–11Fe	−1,220	117.5	92.6	0.00637
Co–25Fe	−1,340	147.1	115.3	0.00373

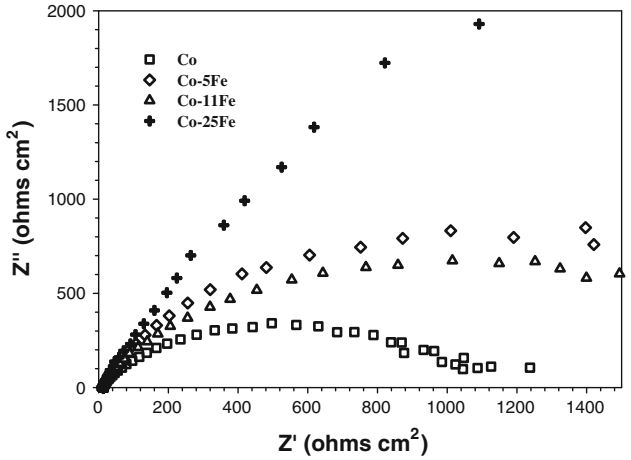

Fig. 14 Nyquist plots for nano Co and CoFe with various iron content in deaerated 0.1 M NaOH

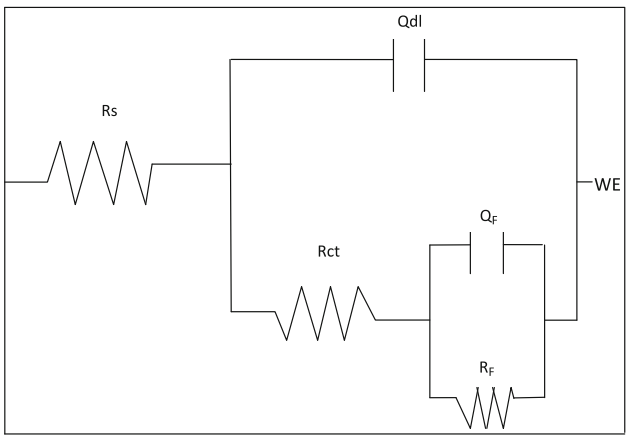

Fig. 15 Equivalent circuit proposed for the electrochemical impedance response of Co and CoFe alloy coatings in 0.1 M NaOH

potential and corrosion current density obtained from the extrapolated cathodic and anodic Tafel line. It can be seen that with an increase in iron content, the corrosion potential (E_{corr}) moved to a more negative potential from −1,080 to −1,340 mV_{SCE}. Furthermore, the corrosion current density (i_{corr}) was also seen to decrease from 6.44×10^{-3} to 3.73×10^{-3} mA cm^{-2} with an increase in Fe content of the alloy coatings. This indicates that reduction in grain size with an increase in Fe content has a significant influence on the passivation behavior of nanocrystalline CoFe

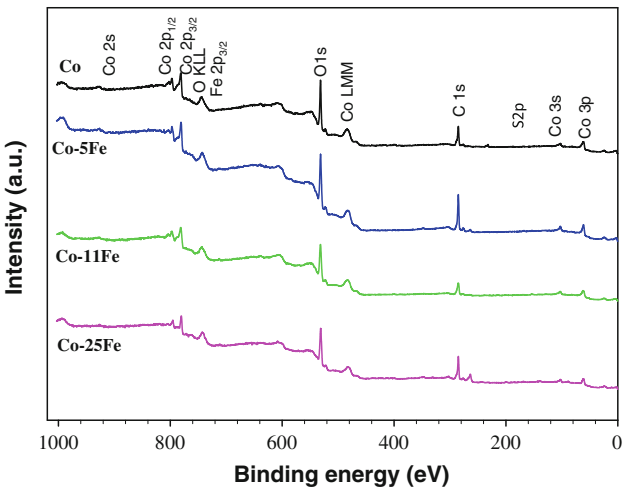

Fig. 16 XPS spectra (full-range) of nano Co and CoFe with various iron content in 0.1 M NaOH

coatings in 0.1 M NaOH. Similar observations of improved corrosion behavior for nanocrystalline materials in alkaline solutions have been reported in several other studies [33–35]. This is due to the high density of nucleation sites present in the CoFe alloy coatings which lead to a rapid formation of a protective passive layer. The formation of a stable passive film increases the difficulty of ions or electrons moving toward the surface to participate in the electrochemical reaction. On the other hand, as all corrosion tests were conducted in deaerated condition, the only possible cathodic reaction is the evolution of hydrogen from water reduction as below:

$$2H_2O + 2e^- \rightarrow 2OH^- + H_2$$

3.3.3 *Electrochemical impedance spectroscopy (EIS) in 0.1 M NaOH*

The Nyquist plots for pure Co and the alloy coatings deposited with different iron contents of 5, 11, and 25 wt% Fe are shown in Fig. 14 for the alkaline solution at −300 mV_{SCE} for 10 min. The investigated electrodes display different frequency responses under the same conditions. The spectra observed exhibited a partially resolved semicircle at high frequencies. Figure 15 shows the

Table 6 EIS data obtained by equivalent circuit simulation in 0.1 M NaOH

Coating	R_s (Ω m^2)	Q_{dl}–Y_o (F cm^{-2})	n_1	R_{ct} (Ω cm^2)	Q_{ct}–Y_o (F cm^{-2})	n_2	R_f (Ω cm^2)
Co	13.37	0.0004763	0.9436	67.78	0.0007561	0.9	1,899
Co–5Fe	11.32	0.0001676	0.8745	71.81	0.0002919	0.5	1,880
Co–11Fe	10.21	0.0006391	0.8533	81.01	0.0001929	0.6	1,856
Co–25Fe	9.58	0.0002812	0.8352	98.93	0.0001065	0.6	2,923

Table 7 Atom concentration ratio (at.%) of elements in XPS analysis for as-deposited samples and polarized in 0.1 M NaOH

Element	As-deposited				Polarized in 0.1 M NaOH			
	Co	Co–5Fe (at.%)	Co–11Fe (at.%)	Co–25Fe (at.%)	Co	Co–5Fe (at.%)	Co–11Fe (at.%)	Co–25Fe (at.%)
Co	9.12	5.87	6.02	1.51	9.67	6.92	9.23	5.18
Fe	–	0.43	0.60	0.82	–	0.53	0.54	0.57
O	23.88	31.00	26.82	13.7	44.21	37.70	43.97	39.63
S	1.01	0.87	0.93	0.22	–	1.05	1.10	0.85

equivalent circuit proposed for the electrochemical impedance response. It consists of a working electrode (W_E), solution resistance (R_s) in series with a double layer capacitance (Q_{dl}), charge transfer resistance (R_{ct}), capacitance of surface film (Q_F), and the surface film resistance (R_F). Table 6 represents the impedance data for Co and CoFe alloy coatings. The solution resistance (R_s) was nearly identical in all cases due to the similar bath chemistry and cell configuration. The surface film resistance (R_F) for the pure Co and CoFe alloy coatings with lower iron content did not have much difference although for the highest iron content alloy, the resistance of passive film was significantly high. The same trend could also be observed for the charge transfer resistance (R_{ct}) where Co 25 wt% Fe results in higher R_{ct} as compared to the other samples. It is obvious that the charge transfer impedance increased with the increase in iron content of the deposits. This indicates that reduction in grain size with high iron content in Co 25 wt% Fe deposit results in higher corrosion resistance as compared to the other coatings.

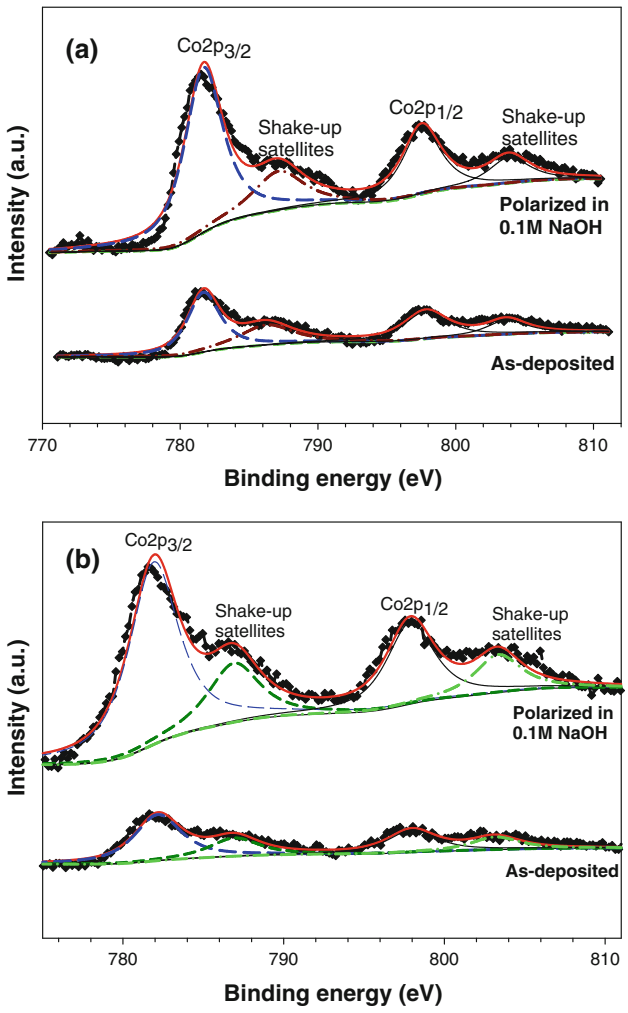

Fig. 17 Comparison of Co 2p peaks of **a** as-deposited Co and Co after polarization in 0.1 M NaOH and **b** as-deposited and Co 25 wt% Fe after polarization in 0.1 M NaOH

3.3.4 X-ray photoelectron spectroscopy analysis

The passive film on Co and CoFe alloy coatings was further analyzed by XPS surface analysis. Figure 16 shows the XPS survey spectrum of pure Co and CoFe alloy coatings after being polarized in NaOH solution which consist of cobalt, oxygen, carbon, sulfur, and iron for the alloy coatings. The XPS spectra for both Co and CoFe alloy coating samples are found to be similar. Table 7 shows the atomic concentration ratio obtained from the XPS survey spectrum. The high-resolution XPS spectra of Co 2p for Co and CoFe alloy are shown in Fig. 17a, b,

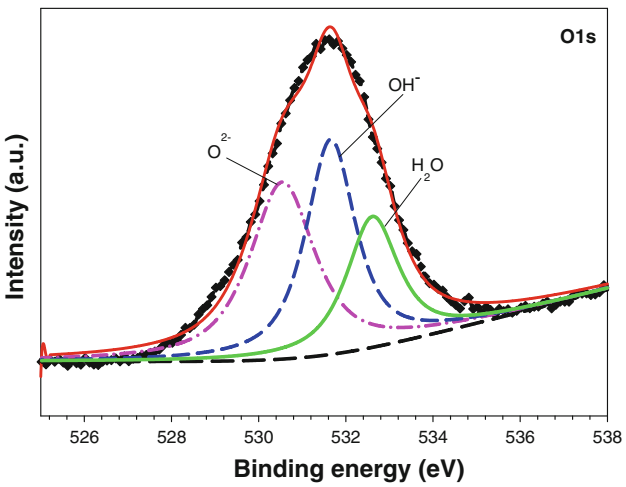

Fig. 18 Measured high-resolution spectra of O 1 s after polarization in 0.1 M NaOH

respectively. Similar to the peaks observed from samples polarized in 0.1 M H_2SO_4, the binding energies of Co doublet peaks of all the samples were around 781.3 ± 0.1 and 798.0 ± 0.1 eV, which represented the $Co(OH)_2$ $2p_{3/2}$ and $Co(OH)_2$ $2p_{1/2}$, respectively [27]. However, two other smaller peaks known as the shake-up satellite peaks were detected at binding energies of 787.4 and 803.3 eV. Furthermore, it is interesting to note that the intensity increased significantly after all samples were polarized. Accordingly, the XPS spectra of O 1 s peak of oxygen were fitted with three peaks at a binding energy of 530.1 ± 0.2 eV corresponding to O^{2-}, 531.4 ± 0.2 eV corresponding to OH^-, and 532.5 ± 0.2 eV corresponding to H_2O, respectively, as shown in Fig. 18 [28]. The water peak is from the surface contamination, and the oxygen peak corresponds to oxygen in $Co(OH)_2$. Results are similar to the XPS peaks observed for coatings studied in acidic solution as discussed earlier. On the other hand, the high-resolution XPS spectrum of Fe 2p is shown in Fig. 19. The spectrum shows two strong peaks of Fe $2p_{3/2}$ and Fe $2p_{1/2}$ at a binding energy of 713.1 and 727.3 eV, respectively, which was found to correspond to the Fe^{3+} ion [29]. The structure splitting of these two components of 14.2 eV is indicative of Fe^{3+} ion that most probably originate from the formation of Fe_2O_3 on the surface of polarized coatings due to oxidation.

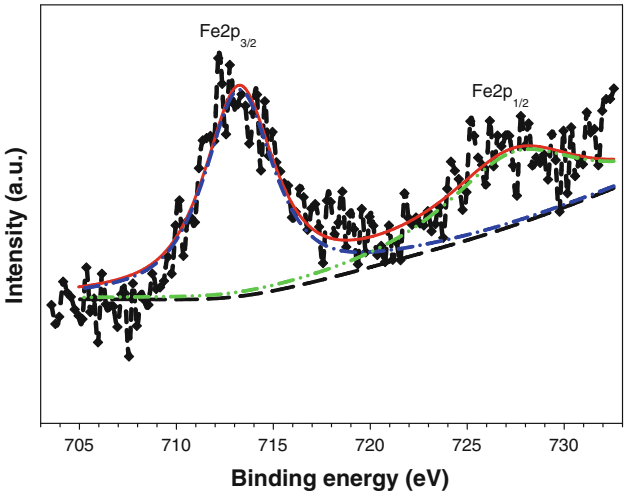

Fig. 19 Measured high-resolution spectra of Fe 2p of the Co 25 wt% Fe alloy coating after polarization in 0.1 M NaOH

3.3.5 *Corrosion morphologies*

The SEM surface morphologies for all samples after potentiodynamic polarization in deaerated 0.1 M NaOH is

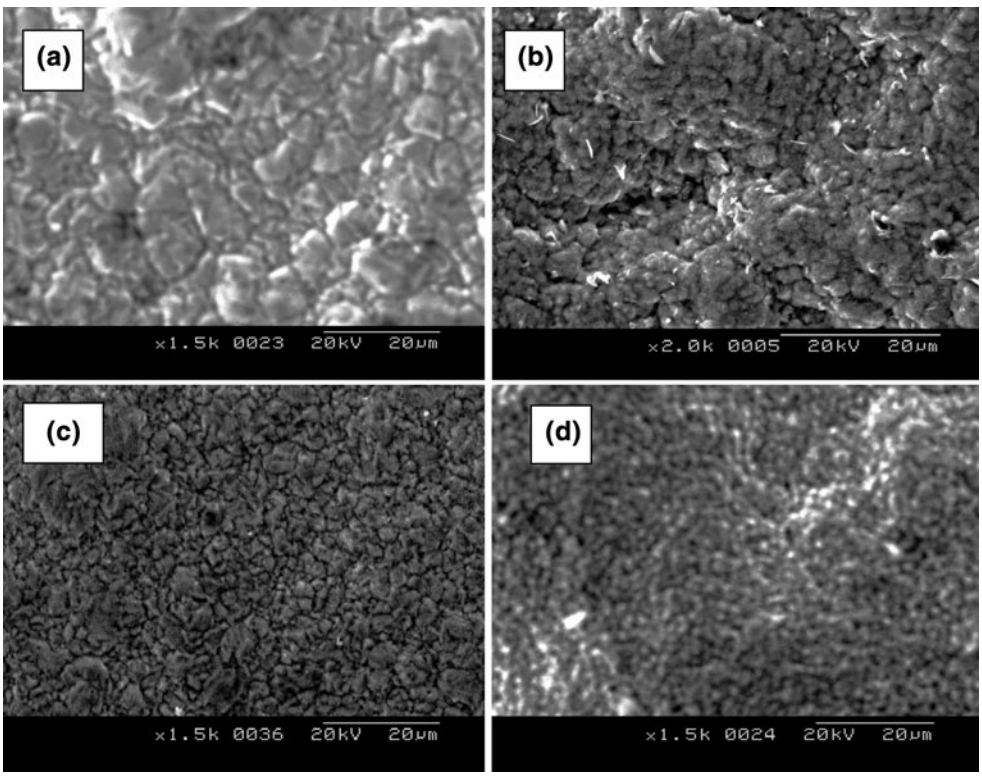

Fig. 20 SEM morphologies of the CoFe alloy coatings after potentiodynamic polarization test in deaerated 0.1 M NaOH **a** Co, **b** Co 5 wt% Fe, **c** Co 11 wt% Fe, **d** Co 25 wt % Fe

shown in Fig. 20. It can be observed that all samples did not exhibit any extensive surface dissolution as were seen from the surface of the corroded samples in acidic solution. The morphologies for both nanocrystalline Co and CoFe appeared to be almost similar. However, finer grains were present in coatings that were alloyed with Fe where an increase in Fe content decreased the grain size of the CoFe alloy deposits. A more dense and smooth surface could be observed on all CoFe alloy coatings where almost no corrosion pits were present. This could be the result of a more protective passive film that was formed on CoFe coatings as compared to pure Co coatings. The effect of reducing the grain size of materials in the nanocrystalline range has resulted in enhanced corrosion resistance behavior as reported by Wang et al. [31] and Luo et al. [36]. In the present study, this effect could also be obviously seen from the potentiodynamic polarization test and was further confirmed by EIS and XPS as well as the surface morphology of the coatings after electrochemical testing indicating that reduced grain size due to iron alloying in CoFe coatings promotes the formation of better passive film resulting in improved corrosion resistance. It is known that passivation is prone to occur on surface nanocrystalline lattice defects [37]. Nanocrystalline CoFe with finer grain sizes as compared to nanorystalline Co is associated with a high volume fraction of intergranular defects such as grain boundaries or triple junctions. Hence, when nanocrystalline CoFe coatings come into contact with the aggressive alkaline solution, the rapid coverage of the passive film on the alloy coating surface largely lowers ions diffusion effect to enhance the resistance to corrosive solution. Therefore, it can be concluded that ultra fine grain size of CoFe alloy coatings enhances the corrosion resistance in 0.1 M NaOH solution.

4 Conclusions

Nanocrystalline Co and CoFe alloy coatings with grain sizes ranging from 60 to 18 nm were synthesized by electrodeposition. The corrosion behavior of nanocrystalline Co and CoFe alloy coatings has been investigated using Tafel plots in both acidic and alkaline solutions. Nanocrystalline Co and CoFe exhibit higher corrosion rates in 0.1 M H_2SO_4 than in alkaline environment. In deaerated acidic solution, both nanocrystalline Co and CoFe alloy coatings exhibit only active anodic dissolution without any passivation. The high volume of grain boundaries for nanocrystalline CoFe due to decrease in grain sizes serve as active surface sites for corrosion reaction which decreases the corrosion resistance in low pH solution. Both nanocrystalline Co and CoFe display a typical active–passive–transpassive behavior with two passivation stages observed in 0.1 M NaOH. Iron alloying did not have any significant effect on the corrosion performance of the alloy coating in the alkaline solution. The two stages of passivation present due to the formation of a duplex passive film.

Acknowledgments Authors are grateful to the Natural Sciences Engineering Research Council of Canada (NSERC). A scholarship granted by Ministry of High Education, Malaysia, and Universiti Teknologi Mara are also gratefully acknowledged.

References

1. Gómez E, Pané S, Vallés E (2005) Electrodeposition of Co–Ni and Co–Ni–Cu systems in sulphate–citrate medium. Electrochim Acta 51:146–153. doi:10.1016/j.electacta.2005.04.010
2. Rashwan SM (2005) Study on the behavior of Zn–Co–Cu alloy electroplating. Mater Chem Phys 89:192–204. doi:10.1016/j.matchemphys.2003.10.019
3. Bajat JB, Petrovic AB, Makimovc MD (2005) Electrochemical deposition and characterization of zinc–nickel alloys deposited by direct and reverse current. J Serb Chem Soc 70:1427–1439. doi:10.2298/JSC0512427B
4. Müller C, Sarret M, Benballa M (2001) Some peculiarities in the codeposition of zinc–nickel alloys. Electrochim Acta 46:2811–2817. doi:10.1016/S0013-4686(01)00493-5
5. Anicai LM, Siteavu, Grunwald E (1992) Corrosion behavior of zinc and zinc alloy depositions. Corros Prev Control 39:89–93. doi:10.1007/BF01024854
6. Alfantazi A, Erb U (1996) Corrosion properties of pulse-plated zinc–nickel alloy coatings. Corrosion 52:880–888. doi:10.5006/1.3292081
7. Jung H, Alfantazi A (2010) Corrosion behavior of nanocrystalline Co and Co-P alloys in a NaOH solution. Corrosion 66:5002. doi:10.5006/1.3360907
8. Jung H, Alfantazi A (2007) Phosphorous alloying and annealing effects on the corrosion properties of nanocrystalline Co-P alloys in acidic solution. Corrosion 63:159–170. doi:10.5006/1.3278340
9. Andricacos PC, Robertson N (1998) IBM J Res Dev 42:671–680. doi:10.1147/rd.425.0671
10. Kohn A, Eizenberg M, Shacham-Diamand Y, Sverdlov Y (2001) Mater Sci Eng A 302:18. doi:10.1063/1.1602572
11. Judy JW, Muller RS, Zappe HH (1995) Magnetic microactuation of polysilicon flexure structures. J Microelectromech Syst 4:162–169. doi:10.1109/84.475542
12. Koza JA, Karnbach F, Uhlemann M, McCord J, Mickel C, Gebert A, Baunack S, Schultz L (2010) Electrocrystallisation of CoFe alloys under the influence of external homogeneous magnetic fields—Properties of deposited thin films. Electrochim Acta 55:819–831. doi:10.1016/j.electacta.2009.08.069
13. Khan H, Petrikowski K (2002) Magnetic and structural properties of the electrochemically deposited arrays of Co and CoFe nanowires. J Magn Mater 249:458–461. doi:10.1016/S0304-8853(02)00453-5
14. Brankovic SR, Bae S, Litvinov D (2008) The effect of Fe3+ on magnetic moment of electrodeposited CoFe alloys—experimental study and analytical model. Electrochim Acta 53:5934–5940. doi:10.1016/j.electacta.2008.03.071
15. Osaka T, Takai M, Sogawa Y, Momma T, Ohashi K, Saito M, Yamada K (1999) Influence of crystalline structure and sulfur inclusion on corrosion properties of electrodeposited CoNiFe soft magnetic films. J Electrochem Soc 146:2092–2096. doi:10.1149/1.1391896

16. Ricq L, Lallemand F, Gigandet MP, Pagetti J (2001) Influence of sodium saccharin on the electrodeposition and characterization of CoFe magnetic film. Surf Coat Technol 138:278–283. doi:10.1016/S0257-8972(00)01170-1
17. Tabakovic I, Riemer S, Tabakovic K, Sun M, Kief M (2006) Mechanism of saccharin transformation to metal sulfides and effect of inclusions on corrosion susceptibility of electroplated CoFe magnetic films. J Electrochem Soc 153:C586–C593. doi:10.1149/1.2207821
18. George J, Rantschler J, Bae SE, Litvinov D, Brankovic SR (2008) Sulfur and saccharin incorporation into electrodeposited CoFe alloys: consequences for magnetic and corrosion properties. J Electrochem Soc 155:D589–D594. doi:10.1149/1.2948377
19. Nik Rozlin NM, Alfantazi AM (2012) Nanocrystalline cobalt–iron alloy: synthesis and characterization. Mater Sci Eng A 550:388–394. doi:10.1016/j.msea.2012.04.092
20. Jung H, Alfantazi A (2006) An electrochemical impedance spectroscopy and polarization study of nanocrystalline Co and Co–P alloy in 0.1 MH_2 SO4 solution. Electrochim Acta 51:1806–1814. doi:10.1016/j.electacta.2005.06.037
21. Jung H, Alfantazi A (2010) Corrosion properties of electrodeposited cobalt in sulfate solutions containing chloride ions. Electrochim Acta 55:865–869. doi:10.1016/j.electacta.2009.09.051
22. Heusler KE (1958) Z Elektrochem 62:582
23. Lallemand F, Ricq L, Berçot P, Pagetti J (2002) Effects of the structure of organic additives in the electrochemical preparation and characterization of CoFe film. Electrochim Acta 47:4149–4156. doi:10.1016/j.surfcoat.2005.01.038
24. Oudar J, Marcus P (1979) Role of adsorbed sulphur in the dissolution and passivation of nickel and nickel-sulphur alloys. Appl Surf Sci 3:48–67. doi:http://dx.doi.org/10.1016/0378-5963(79)90060-6
25. Keddam M, Mottos OR, Takenouti H (1981) Reaction model for iron dissolution studied by electrode impedance I. Experimental results and reaction model. J Electrochem Soc 128:257–266. doi:10.1149/1.2127402
26. Parthasarathi B, Seenivasan H, Rajam KS, Grips VKW (2012) Characterization of amorphous Co–P alloy coatings electrodeposited with pulse current using gluconate bath. Appl Surf Sci 258:9544–9553. doi:10.1016/j.apsusc.2012.05.115
27. Tan BJ, Klabunde KJ, Sherwood PMA (1991) XPS studies of solvated metal atom dispersed (SMAD) catalysts. Evidence for layered cobalt-manganese particles on alumina and silica. J Am Chem Soc 113:855–861. doi:10.1021/ja00003a019
28. Tsutsumi Y, Nishimura D, Doi H, Nomura N, Hanawa T (2010) Cathodic alkaline treatment of zirconium to give the ability to form calcium phosphate. Acta Biomater 6:4161–4166. doi:10.1016/j.actbio.2010.05.010
29. McIntyre NS, Zetaruk DG (1977) Anal Chem 49:1521–1529. doi:10.1021/ac50019a016
30. Rofagha R, Erb U, Ostrander D, Palumbo G, Aust K (1993) The effects of grain size and phosphorus on the corrosion of nanocrystalline Ni–P alloys. Nanostruct Mater 2:1–10. doi:10.1016/0965-9773(93)90044-C
31. Wang L, Lin Y, Zeng Z, Liu W, Xue Q, Hu L, Zhang J (2007) Electrochemical corrosion behavior of nanocrystalline Co coatings explained by higher grain boundary density. Electrochim Acta 52:4342–4350. doi:10.1016/j.electacta.2006.12.009
32. Ives DJG, Rawson AE (1962) Copper corrosion III. Electrochemical theory of general corrosion. J Chem Soc 109:447–466. doi:10.1149/1.2425447
33. Youssef KMS, Koch C, Fedkiw P (2004) Influence of additives and pulse electrodeposition parameters on production of nanocrystalline zinc from zinc chloride electrolytes. J Electrochem Soc 151:C103–C111. doi:10.1149/1.1636739
34. Shriram S, Mohan S, Renganathan N, Venkatachalam R (2000) Electrodeposition of nanocrystalline nickel: a brief review. Trans Inst Met Finish 78:194–197
35. Inturi R, Szklarska-Smialowska Z (1992) Localized corrosion of nanocrystalline 304 type stainless steel films. Corrosion 48:398–403. doi:0010-9312/92/000091
36. Luo W, Xu Y, Wang Q, Shi P, Yan M (2010) Effect of grain size on corrosion of nanocrystalline copper in NaOH solution. Corros Sci 52:3509–3513. doi:10.1016/j.corsci.2010.06.029
37. Balyanov A, Kutnyakova J, Amirkhanova N, Stolyarov V, Valiev R, Liao X, Zhao Y, Jiang Y, Xu H, Lowe T (2004) Corrosion resistance of ultra fine-grained Ti. Scr Mater 51:225–229. doi:10.1016/j.scriptamat.2004.04.011